China Geology 7 (2024) 188–202

China Geology

Journal homepage: http://chinageology.cgs.cn
https://www.sciencedirect.com/journal/china-geology

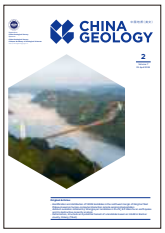

Spatial structural characteristics of the Deda ancient landslide in the eastern Tibetan Plateau: Insights from Audio-frequency Magnetotellurics and the Microtremor Survey Method

Zhen-dong Qiu[a, b], Chang-bao Guo[a, c, d,*], Yi-ying Zhang[a, e], Zhi-hua Yang[a, c, d], Rui-an Wu[a, c, d], Yi-qiu Yan[a], Wen-kai Chen[a], Feng Jin[a]

[a] *Institute of Geomechanics, Chinese Academy of Geological Sciences, Beijing* 100081, *China*
[b] *Faculty of Engineering, China University of Geosciences, Wuhan* 430074, *China*
[c] *Key Laboratory of Active Tectonics and Geological Safety, Ministry of Natural Resources, Beijing* 100081, *China*
[d] *Research Center of Neotectonism and Crustal Stability, China Geological Survey, Beijing* 100081, *China*
[e] *China Water Resources Beifang Investigation, Design and Research Co. Ltd., Tianjin* 300222, *China*

ARTICLE INFO

Article history:
Received 8 November 2023
Received in revised form 12 February 2024
Accepted 20 February 2024
Available online 23 February 2024

Keywords:
Ancient landslide
Remote sensing
Audio-frequency Magnetotellurics (AMT)
Microtremor Survey Method (MSM)
Geological drilling engineering
Spatial structure
Tibetan Plateau
Geological hazard survey engineering

ABSTRACT

It is of crucial importance to investigate the spatial structures of ancient landslides in the eastern Tibetan Plateau's alpine canyons as they could provide valuable insights into the evolutionary history of the landslides and indicate the potential for future reactivation. This study examines the Deda ancient landslide, situated in the Chalong-ranbu fault zone, where creep deformation suggests a complex underground structure. By integrating remote sensing, field surveys, Audio-frequency Magnetotellurics (AMT), and Microtremor Survey Method (MSM) techniques, along with engineering geological drilling for validation, to uncover the landslide's spatial features. The research indicates that a fault is developed in the upper part of the Deda ancient landslide, and the gully divides it into Deda landslide accumulation zone I and Deda landslide accumulation zone II in space. The distinctive geological characteristics detectable by MSM in the shallow subsurface and by AMT in deeper layers. The findings include the identification of two sliding zones in the Deda I landslide, the shallow sliding zone (DD-I-S1) depth is approximately 20 m, and the deep sliding zone (DD-I-S2) depth is 36.2–49.9 m. The sliding zone (DD-II-S1) depth of the Deda II landslide is 37.6–43.1 m. A novel MSM-based method for sliding zone identification is proposed, achieving less than 5% discrepancy in depth determination when compared with drilling data. These results provide a valuable reference for the spatial structural analysis of large-deep-seated landslides in geologically complex regions like the eastern Tibetan Plateau.

1. Introduction

Ancient landslides refer to landslides that occurred before the Holocene and have undergone a long-term complex evolutionary process (Cruden DM and Varnes DJ, 1996). These landslides reactivated along foregone sliding surfaces and also can generate new secondary landslides, presenting deformation characteristics of multi-periods, multi-zones, and multi-level sliding zones (Li X et al., 2008; Zhang YS et al., 2015; Guo CB et al., 2022). In the eastern Tibetan Plateau, where the topography has the steepest slopes and tectonic activities are the most intense (Dewey JF et al., 1988; Peng JB et al., 2004; Xu JR and Zhao ZX, 2009; Yang ZH et al., 2023), large ancient landslides induced by both internal and external geological processes are widely distributed, such as the Luanshibao landslide (Guo CB et al., 2016), Jiangdingya ancient landslide (Guo CB et al., 2023), and Xiongba ancient landslide (Guo CB et al., 2021). Due to the complex topographical and geological conditions as well as poor transportation in the eastern Tibetan Plateau, the spatial structural characteristics of large ancient landslides in alpine canyon areas has always been a focal point and challenge in geological hazard research.

The current investigation of large ancient landslides in the

First author: *E-mail address*: qiuzhendong@cug.edu.cn (Zhen-dong Qiu).

* Corresponding author: *E-mail address*: guochangbao@cags.ac.cn (Chang-bao Guo).

Literary editor: Xi-jie Chen
doi:10.31035/cg2023129
2096-5192/© 2024 China Geology Editorial Office.

eastern Tibetan Plateau's alpine canyons primarily employs a combination of methods including remote sensing interpretation, unmanned aerial vehicle (UAV), and field surveys to ascertain the surface development characteristics of the landslides (Yan YQ et al., 2022; Xu Q et al., 2023). Techniques such as geophysical exploration and engineering geological drilling are utilized to ascertain the spatial structural development features of the landslides (Le Roux O et al., 2011). In recent years, numerous scholars both domestically and internationally have conducted extensive research on the spatial structure features of landslides using geophysical exploration techniques. Among these, based on the electrical differences in various rock types, techniques such as High-density Electrical Resistivity, Electrical Resistivity Tomography, and Audio-frequency Magnetotellurics are used to determine landslide body thickness, sliding zone depth, groundwater-rich zones, crack extensions, and fault distributions (Yang DD et al., 2021; Yang XH et al., 2023). Additionally, based on the differences in wave velocities in different rock types, surface wave exploration techniques such as Refraction Seismic Method, Reflection Seismic Method, and Rayleigh Surface Wave Method are employed to identify the characteristics of boulder distribution and stratification of formations (Gao WW et al., 2018; Xu PF et al., 2021). By comprehensively employing geophysical methods to identify the underground spatial structure of landslides, combined with validation through engineering geological drilling and field investigations, the developmental characteristics of landslides can be accurately identified (Naudet V et al., 2008; Su LJ et al., 2017; Ma N et al., 2019).

The Deda ancient landslide in Deda Township, Batang County, Sichuan Province, is located within the Chalong-ranbu fault zone. Previous investigations have suggested that it has been significantly affected by active faults and river erosion, displaying signs of reactivation and deformation (Zhang YY et al., 2021; Zhang LQ, 2017). This landslide is representative of the region, but the spatial structure and the characteristics of the deep sliding zone remain unclear. The developmental features and stability of this landslide have a significant impact on the safety of infrastructure such as major railway projects, important transportation routes and significant villages constructed at its forefront. In this study, a combination of remote sensing interpretation, UAV surveys, field investigations, AMT, MSM, and engineering geological drilling were employed to investigate the developmental characteristics in the Deda ancient landslide. The spatial structural developmental features of the Deda ancient landslide were identified, and a sliding zone identification method based on MSM was proposed. The research findings hold significant reference value for understanding the stability and development trends of the Deda ancient landslide. The research methods provide important guidance for the study of the mechanisms and stability of large ancient landslides in the alpine canyon area of the eastern Tibetan Plateau.

2. Geological background

The Deda ancient landslide is located in Zhongdeda Village, Deda Township, Batang County, Sichuan Province, on the right bank of the Baqu River, with geographic coordinates of approximately 99°24′40″E, 30°18′09″N (Fig. 1), on the eastern part of Tibetan Plateau. The Batang County is located in the semi-humid climate zone, with elevations ranging from 2240 m to 6060 m. The region falls within the extremely high mountain subzone on the eastern bank of the Jinsha River in the "Western Sichuan high mountains and plateau" landform. The rainfall is concentrated primarily from June to September, with an average annual precipitation of 436 mm. The Deda landslide, Zhama landslide, and Jiexieleba landslide developed along the Baqu River (Zhang YY et al., 2021).

The study area is situated in the transitional zone of the arcuate tectonic belt on the eastern edge of the Tibetan Plateau. The Hengduan Mountains traverse the entire region, with active and intense tectonic movements, mainly characterized by pronounced differential uplift and horizontal compression (Wu RA et al., 2023). According to the Seismic Ground Motion Parameters Zonation Map of China (GB 18306-2015), the seismic intensity in the landslide area is categorized as Zone VIII. Historically, the region has experienced three earthquakes with a magnitude of $M_S \geqslant 6.0$ (Zhou RJ et al., 2005). The main lithological formations exposed in the Deda ancient landslide area are the sandy slate and slate of the Middle-Lower Triassic Cigang Group ($T_{1\text{-}2}{}^{b}$) and limestone of the Upper Triassic Qugasi Formation (T_3q^{l}).

3. Methods

The remote sensing interpretation, UAV surveys, field investigations, geophysical prospecting techniques, and engineering geological drilling were carried out in this study to figure out the spatial structural characteristics of the Deda ancient landslide (Fig. 2).

3.1. Geological survey

The high resolution Google Earth remote sensing images were utilized to identify surface deformations, interpret morphological characteristics, and delineate the scope of potential hazards in the Deda ancient landslide. High-precision remote sensing images were acquired through UAV surveys. Concurrently, field verification was conducted to understand the surface deformation characteristics of the Deda ancient landslide. Subsequently, the locations for deploying geophysical prospecting profiles were determined. Finally, engineering geological drilling positions were figured out based on the geophysical prospecting results (Fig. 2). The geophysical exploration in this project utilizes two methods: Audio-frequency Magnetotellurics (AMT) and the Microtremor Survey Method (MSM). The drilling operation employs the GY-200 high-speed hydraulic drilling rig, utilizing the double-tube single-action drilling technique for

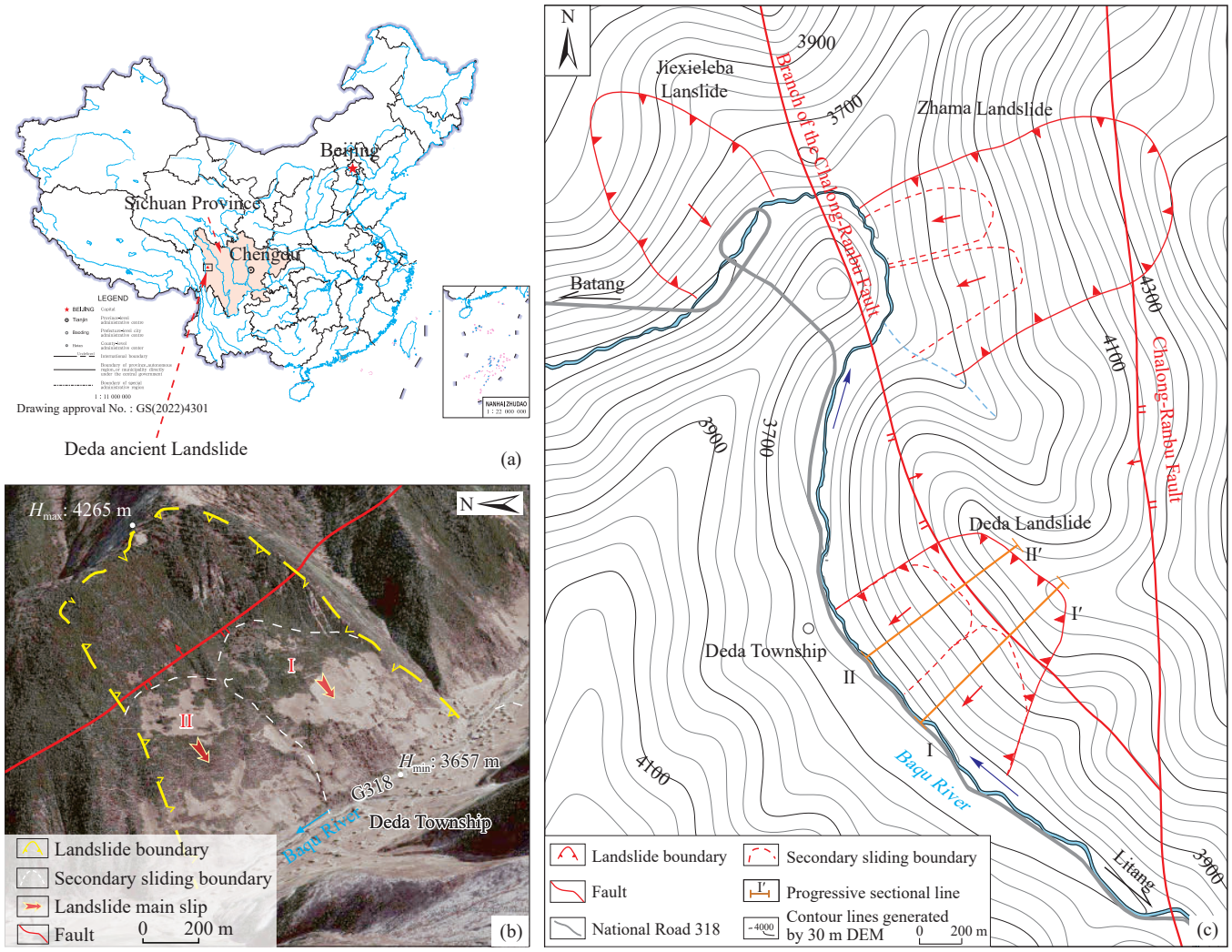

Fig. 1. Spatial location map of the Deda ancient landslide in Batang County, Sichuan Province. a–location map of the Deda ancient landslide study area; b–remote sensing images interpretation of the Deda ancient landslide (base map after Google Earth); c–fault structure distribution characteristics around the Deda township.

on-site drilling. The final hole condition is achieved when drilling reaches the intact bedrock at a depth of 10 m.

3.2. Audio-frequency Magnetotellurics (AMT)

3.2.1. Principles of AMT

AMT is a geophysical prospecting technique based on electromagnetic induction theory, initially proposed by Cagniard L (1953) and Tikhonov AN (1950). The fundamental principle involves transforming electromagnetic information in the time domain into spectral information in the frequency domain. Based on the spectral analysis results, parameters such as E_x, E_y, H_x, H_y are obtained, followed by the derivation of tensors, apparent resistivity, etc. (Di QY et al., 2020).

$$Z_{xy} = \frac{E_x}{H_y} = \sqrt{-i\omega\mu\rho}, Z_{yx} = \frac{E_y}{H_x} = -\sqrt{-i\omega\mu\rho} \quad (1)$$

Furthermore $|Z_{xy}| = |Z_{yx}| = |Z|$, in Eq. 1, Z represents the tensor impedance, E_x and E_y are observed electric field components, H_x and H_y are magnetic field components, i is the imaginary unit, ω is the angular frequency, μ is magnetic permeability, and ρ is electrical resistivity.

The relationship between resistivity and wave impedance of the medium:

$$\rho = \frac{|Z|^2}{\omega\mu} = \frac{|Z|^2}{5f} \quad (2)$$

In Eq. 2, ρ represents electrical resistivity, Z denotes tensor impedance, ω is angular frequency, μ stands for magnetic permeability, and f represents frequency.

3.2.2. Acquisition and inversion of AMT data

The depth at which the amplitude attenuates to the amplitude value at the ground surface in the propagation of subsurface media is referred to as the skin depth or penetration depth, denoted by δ:

$$\delta = 503\sqrt{\frac{\rho}{f}} \quad (3)$$

In Eq. 3, ρ represents the electrical resistivity of the

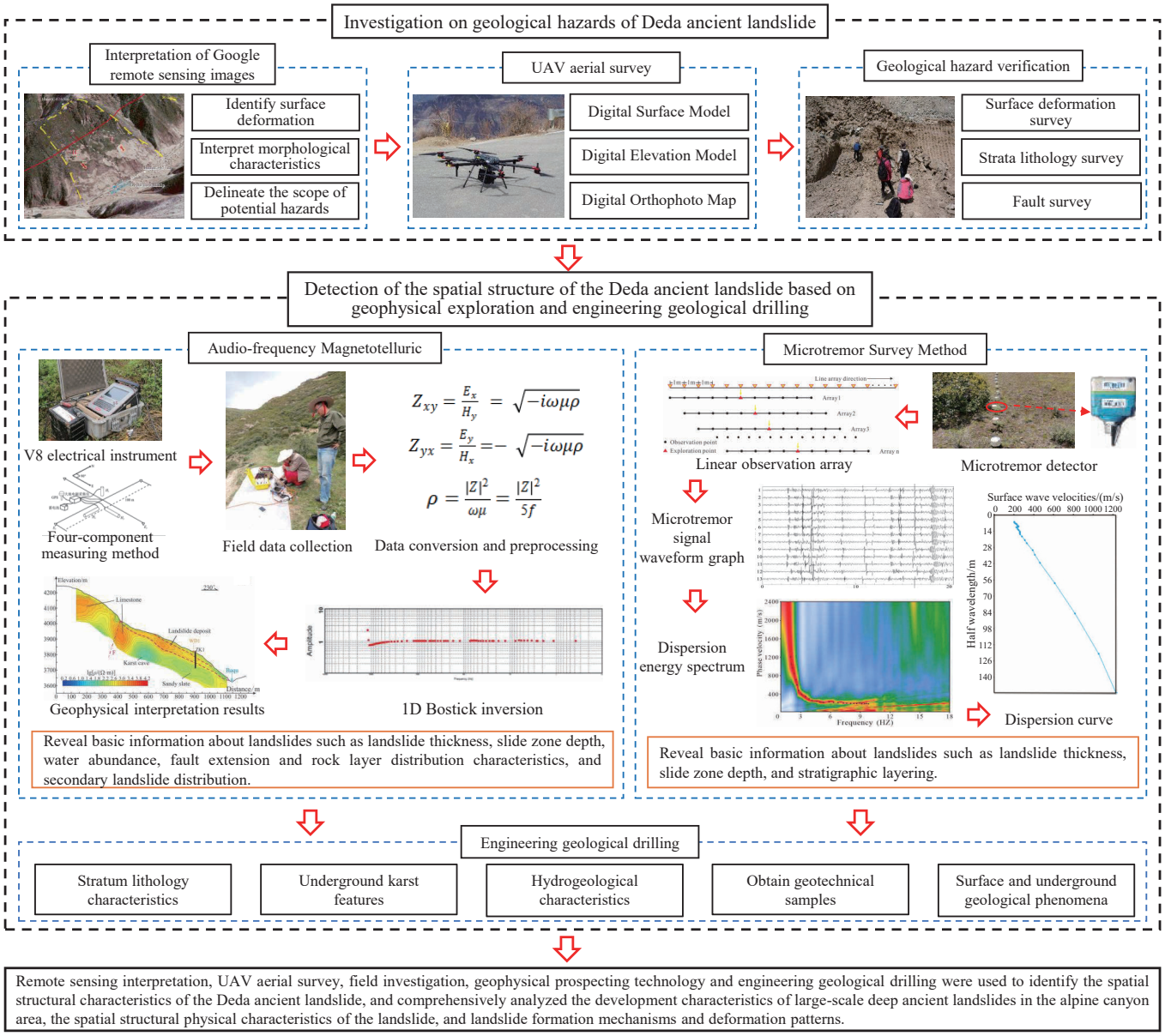

Fig. 2. Flow chart of the spatial structure analysis of the Deda landslide.

subsurface media, and f signifies the frequency of the electromagnetic field.

For the field data acquisition of the AMT survey was conducted using the V8 multifunctional electrical instrument by Phoenix Geophysics, Canada. Data processing and inversion utilized the MTSoft2D series software developed by Chengdu University of Technology. In this AMT data inversion, a one-dimensional Bostick inversion was used to establish the initial model, followed by a two-dimensional inversion using Non-linear Conjugate Gradient (NLCG). This inversion technique effectively revealed geological features such as strata structures and fault distributions (Zhang SL et al., 2021; Yu PL et al., 2023).

3.3. Microtremor Survey Method (MSM)

3.3.1. Principles of MSM

The MSM was put forward by American geophysicists Aki K (1957) and Capon J (1969). It relies on the dispersive properties of Rayleigh waves in seismic surface waves. Specifically, when Rayleigh waves encounter heterogeneous media, their phase velocity varies with frequency (Molnar S et al., 2022). The fundamental principle involves extracting the dispersion curve of Rayleigh waves from microtremor signals collected in the field. Subsequently, by inversion, the shear wave velocity is obtained and utilized to interpret the spatial distribution characteristics of subsurface geology.

3.3.2. Acquisition and inversion of MSM

The methods to extract dispersion curves from microtremor signals include Spatial Autocorrelation method (SPAC) (Aki K, 1957), Frequency-Wavenumber method (F-K) (Capon J, 1969), Refraction Microtremor method (ReMi) (Louie JN and Faster B, 2001), Extended Spatial Autocorrelation (ESPAC) method (Okada H and Suto K, 2003), among others. An A1-3C triaxial microtremor

instrument was employed, and a linear observation array was set up using the commonly used Spatial Autocorrelation method (SPAC) in this study (Fig. 2). The observation array consisted of 33 seismometers. Following data acquisition, dispersion curves of Rayleigh waves were extracted from the microtremor signals. The spatial autocorrelation coefficient, defined as the angular frequency:

$$\rho(\omega,r) = \mathrm{J}_0(rk) \tag{4}$$

$$\rho(\omega,r)=\frac{1}{2\pi}\int_0^{2\pi}\frac{\mathrm{Re}[S_{ox}(\omega,r,\theta)]}{\sqrt{S_o(\omega)\cdot S_x(\omega,r,\theta)}}d\theta \tag{5}$$

In Eq. 4, $\mathrm{J}_0(rk)$ represents the zeroth-order Bessel function of the first kind, and rk is the argument. In Eq. 5, $\mathrm{S}_o(\omega)$ and $\mathrm{S}_x(\omega,\mathrm{r},\theta)$ represent the power spectra of micro-motion data at the array center O and on the circumference, respectively. $\mathrm{S}_{ox}(\omega,\mathrm{r},\theta)$ denotes the cross-power spectrum between the point O at the center and the point X on the circumference. (You ZW et al., 2022). The spatial autocorrelation coefficients were obtained for different ω values. After azimuthal averaging and fitting with the zeroth-order Bessel function of the first kind, Rayleigh wave propagation velocities $\mathrm{c}(\omega)$ at different frequencies were derived, thereby obtaining the dispersion curve of Rayleigh waves.

The extracted dispersion curves are inverted using a damped least squares method to obtain the corresponding shear wave velocity structure. By combining data from multiple measurement points, the shear wave velocity profile for the entire survey line can be obtained. This allows for the analysis of the spatial distribution characteristics of the subsurface (Tian BQ et al., 2019).

4. Development characteristics of Deda ancient landslide

4.1. Analysis of planar characteristics of Deda ancient landslide

The planar morphology of the Deda ancient landslide exhibits a dustpan shape, characterized by a steep-moderate-steep in the topography. The rear elevation of the landslide is 4265 m, while the elevation of the Baqu River is 3657 m, resulting in a relative height difference of 608 m between the front and back edges of the landslide. The boundaries are defined by the bedrock on both sides, the Baqu River at the front, and the ridge at the back. The landslide has a longitudinal length of approximately 1200 m, a transverse width of 1100 m, and an approximate planar area of 1.32×10^6 m^2. The average slope ranges from 20° to 45°, and the orientation of the slope is approximately between 230° and 250°. Based on the planar distribution characteristics of the Deda ancient landslide, it can be divided into three parts: The Deda landslide accumulation zone I, the Deda landslide accumulation zone II and the source zone of the Deda ancient landslide (III) (Fig. 3a).

4.1.1. Deda landslide accumulation zone I

Deda landslide accumulation zone I is developed on the left side of the landslide, presenting a dustpan shape (Fig. 4a). The elevation of the landslide body ranges from 3657 m to

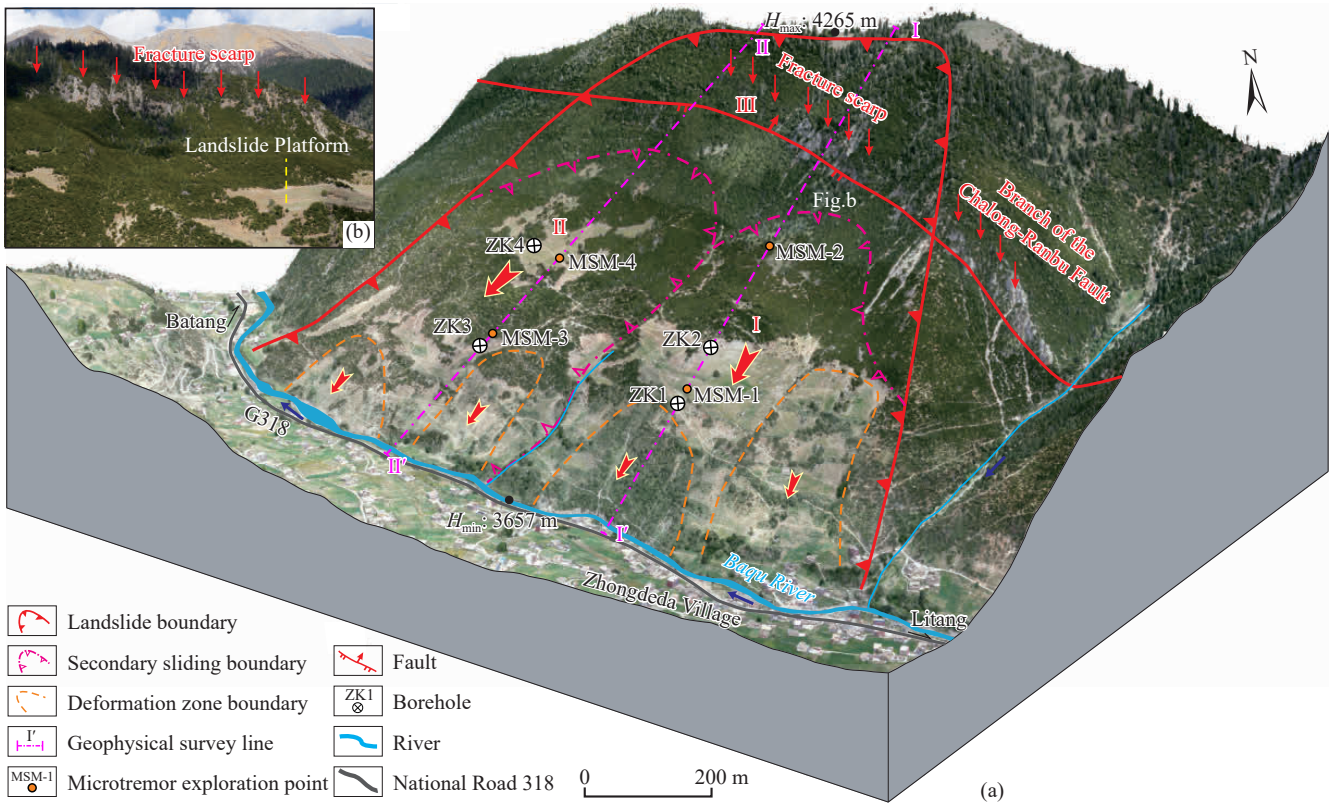

Fig. 3. 3D geological model of the Deda ancient landslide. a–the UAV remote sensing interpretation and engineering survey deployment map of the Deda ancient landslide; b–the rear edge fracture scarp of Deda ancient landslide (mirror to NE).

4000 m, with a longitudinal length of approximately 480 m and a transverse width of approximately 500 m. The planar area is approximately 24×10^4 m^2. The left boundary of the accumulation is marked by a steep rocky scarp, the right boundary is defined by a gully, and the back edge features a fault scarp reaching approximately 200 m in height. The front edge is delineated by the Baqu River, and the main sliding direction is 230°. The upper part of Deda landslide accumulation zone I develops tensional cracks (Fig. 4b), with the development of two resurgent deformation zones at the front edge. There is also a multi-stage sliding phenomenon influenced by erosion from Baqu. Currently, sliding deformation is still occurring.

4.1.2. Deda landslide accumulation zone II

Deda landslide accumulation zone II is situated on the right side of the landslide, displaying an armchair shape. The elevation of the landslide body ranges from 3660 m to 4010 m, with a longitudinal length of approximately 570 m and a transverse width of approximately 440 m. The planar area covers an approximate area of 25×10^4 m^2. The right boundary of the accumulation is marked by a steep rocky scarp, the left boundary is a gully, and the back edge is delineated by a fault scarp reaching approximately 150 m in height. The front edge is defined by the Baqu River, and the main sliding direction is 240°. The Deda landslide accumulation zone II exhibits two reactivation zones at the front edge, where multiple small-scale sliding events occur within these zones, and some of these slide areas impact the river channel (Fig. 4c).

4.1.3. Source zone of the Deda ancient landslide (III)

The elevation of the rear edge of the landslide ranges from 4000 m to 4265 m. The rear edge can be seen as a distinctly fault scarp, with a height of 150 m to 200 m. The bedrock can be seen to be exposed (Fig. 3b, Fig. 4d), and the lithology is limestone. According to regional geological information, a branch of the Chalong-ranbu fault zone traverses through the source zone of the landslide. The front of the fault scarp constitutes the landslide accumulation platform (Fig. 3b).

4.2. Spatial structural characteristics of Deda landslide accumulation zone I

Based on the comprehensive field investigation, two geophysical prospecting lines, designated I-I' and II-II' (Fig. 3a), were set up on the Deda ancient landslide. These survey lines utilized AMT and MSM to explore the subsurface spatial structure. MSM-1, MSM-2, MSM-3 and MSM-4 are four microtremor exploration points arranged within the landslide deposit on two MSM profiles (Fig. 3a). Comprehensive analysis of the spatial structure response characteristics of the Deda ancient landslide in geophysical techniques.

4.2.1. Results of AMT of Deda landslide accumulation zone I

Based on the AMT results (Fig. 5a), it is evident that there are two sliding zones in Deda ancient landslide zone I. The shallow sliding zone can reach a maximum depth of 34.7 m with an average thickness of 20 m, while the deep sliding zone can reach a maximum depth of 73.5 m with an average thickness of 50 m.

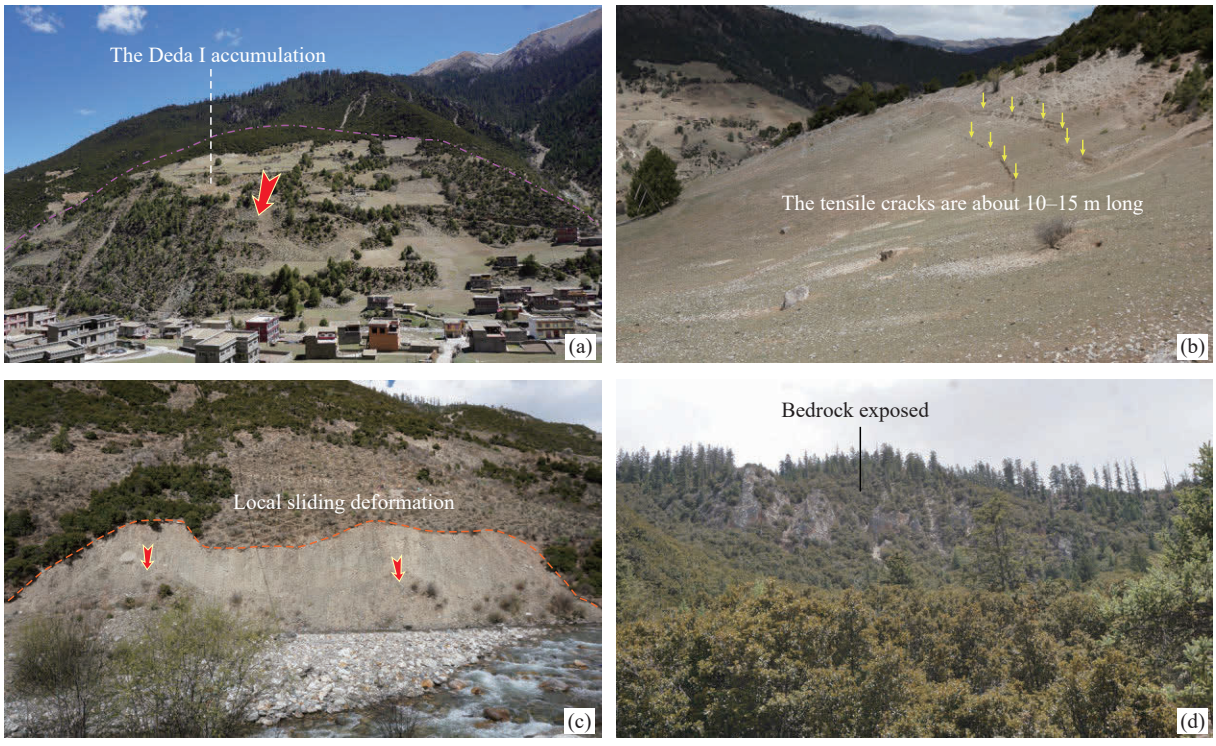

Fig. 4. Development characteristics of the Deda ancient landslide. a–morphological characteristics of the Deda I accumulation (mirror to N); b–the tension cracks developed in the Deda I accumulation (mirror to NW); c–Deda ancient landslide front reactivation deformation (mirror to NE); d–bedrock exposed at the rear edge of the landslide (mirror to NE).

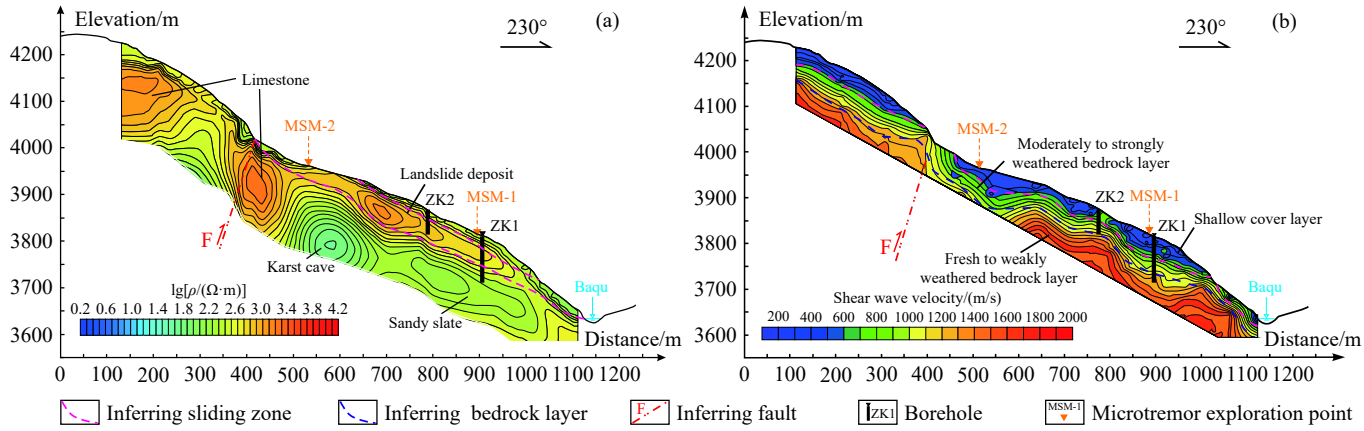

Fig. 5. Two-dimensional physical response characteristics of the I-I' sections of the Deda ancient landslide. a–inversion results of AMT in the I-I' section of the Deda ancient landslide; b–inversion results of MSM in the I-I' section of the Deda ancient landslide.

The resistivity of the sliding body varies in the range of 100–1258.9 Ω·m, primarily composed of gravel soil. Below the landslide is the bedrock, exhibiting a significant increase in resistivity, reaching 3162 Ω·m. Considering the geological data in this area, it is inferred that the high resistivity zone in the middle and rear parts of the landslide is characteristic of limestone. Locally, within the deep bedrock layers, there are areas with low resistivity ranging from 10 Ω·m to 251 Ω·m, indicating potential karst features in the limestone area. In addition, due to intense tectonic activity in the region, there is extensive development of fractures within the rock mass, including joint fracture surfaces. Therefore, deep within the layers, there may be the flow of karst fissure water. Additionally, a distinct high-low resistivity zone is observed in the middle to rear part of the landslide, suggesting a probable branch fault of the Chalong-ranbu fault traversing the region.

4.2.2. Results of MSM of Deda landslide accumulation zone I

According to the MSM (Fig. 5b) and a comprehensive analysis of microtremor exploration points MSM-1 and MSM-2 (Fig. 6), the spatial structure of the Deda ancient landslide zone I can be categorized into three layers: (1) shallow cover layer; (2) moderately to strongly weathered bedrock layer; (3) fresh to weakly weathered bedrock layer.

(i) Data analysis of the microtremor exploration point MSM-1 located in the middle of the Deda I accumulation reveals the following (Fig. 6c):

Shallow cover layer: The shear wave velocity in this layer ranges from 200.0 m/s to 644.2 m/s, mainly consisting of loose gravel soil, with a thickness of approximately 47.3 m.

Moderately to strongly weathered bedrock layer: The shear wave velocity in this layer falls between 644.2–766.0 m/s, indicating moderately to strongly weathered bedrock. It is situated at a depth of 47.3–67.8 m with a thickness of approximately 20.5 m.

Fresh to weakly weathered bedrock layer: The shear wave velocity in this zone ranges from 766.0 m/s to 1206.1 m/s, representing fresh to weakly weathered bedrock. The rock mass shows good integrity and a compact structure at a depth of 67.8–120.0 m with a thickness of approximately 52.2 m.

Significant differences in shear wave velocity structure are observed at depths of 20.1 m and 47.3 m, with velocity changes of 116.5 m/s and 121.7 m/s, respectively. These locations are speculated to be potential sliding zones, with a shear wave velocity of 349.5 m/s for the shallow sliding zone and 644.2 m/s for the deep sliding zone.

(ii) Data analysis of the microtremor exploration point MSM-2 located in the rear part of the Deda I accumulation reveals the following (Fig. 6f):

Shallow cover layer: The shear wave velocity in this layer ranges from 203.7 m/s to 553.6 m/s, consisting mainly of loose fragmented rocks with a thickness of 36.2 m.

Moderately to strongly weathered bedrock layer: The shear wave velocity in this layer falls between 553.6–749.2 m/s, indicating moderately to strongly weathered bedrock. It is situated at a depth of 36.2–54.7 m with a thickness of approximately 18.5 m.

Fresh to weakly weathered bedrock layer: The shear wave velocity in this zone ranges from 749.2 m/s to 1060.7 m/s, representing fresh to weakly weathered bedrock. The rock mass shows good integrity and a compact structure at a depth of 54.7–100.0 m with a thickness of approximately 45.3 m.

A significant difference in shear wave velocity structure is observed at a depth of 36.2 m, with a velocity change of 130.8 m/s, indicating a potential sliding zone. The shear wave velocity of this sliding zone is 553.6 m/s.

In summary, MSM-1 reveals two sliding zones with burial depths of approximately 20.1 m and 47.3 m, while MSM-2 reveals one sliding zone with a burial depth of 36.2 m. It is speculated that the deep sliding zone of Deda I landslide accumulation body has a burial depth of 36.2–47.3 m, with a shear wave velocity of 553.6–644.2 m/s. The shallow sliding zone in the central front part has a burial depth of approximately 20 m, with a shear wave velocity of 349.5 m/s.

Toward the rear of the shear wave velocity inversion profile (Fig. 5b), distinct high-low velocity areas are visible, likely indicative of a branch fault of the Chalong-ranbu fault within the region. This distribution aligns with the findings from the AMT, providing consistent results.

4.2.3. Results of engineering geological drilling of Deda

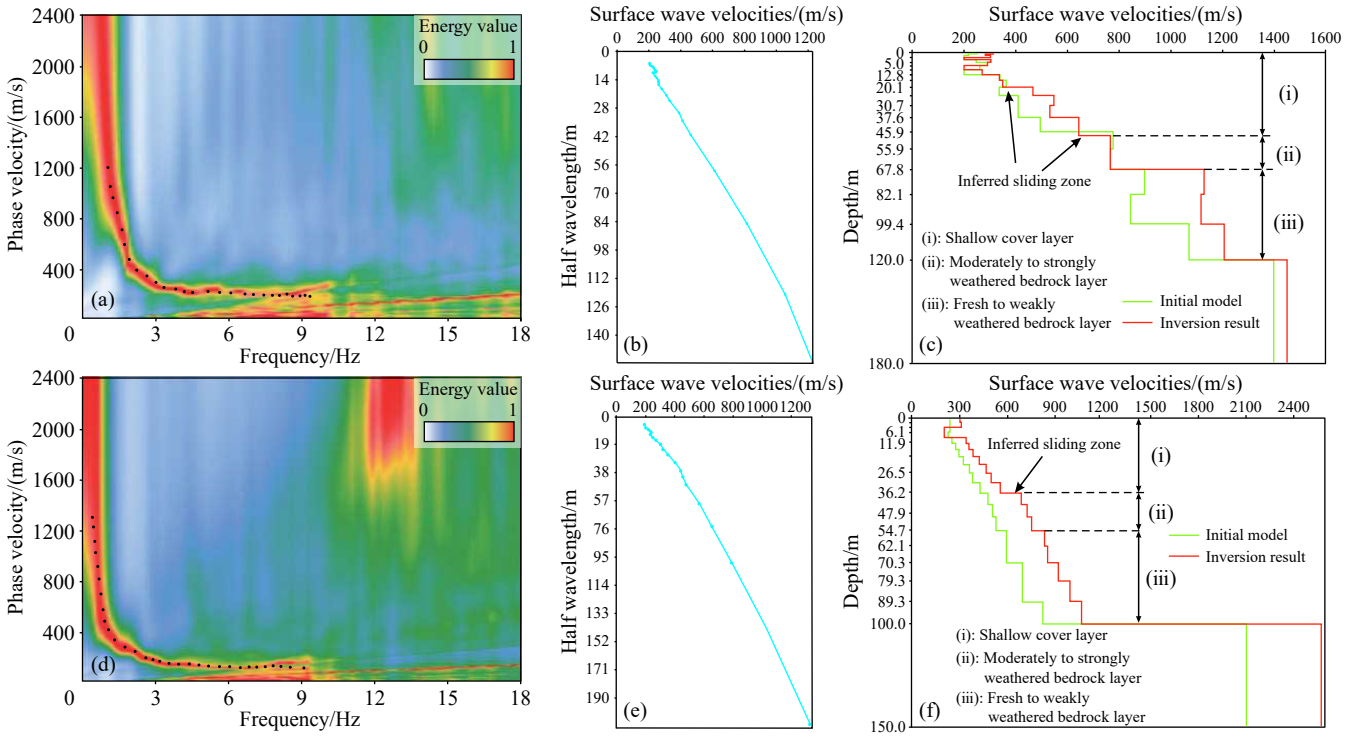

Fig. 6. Geophysical response characteristics of microtremor exploration points on Deda I landslide. a–MSM-1 dispersion energy spectrum; b–MSM-1 dispersion curve; c–inversion of MSM-1 shear wave velocity structure; d–MSM-2 dispersion energy spectrum; e–MSM-2 dispersion curve; f–inversion of MSM-2 shear wave velocity structure.

landslide accumulation zone I

For the Deda landslide accumulation zone I, borehole ZK1 and ZK2 were arranged in the middle of the sliding accumulation body to validate the results of geophysical exploration. And a detailed discussion of ZK1 is conducted in conjunction with the geophysical exploration results (Fig. 3a, Fig. 7).

According to the drilling results of ZK1 (Fig. 7), the Quaternary alluvial layer with a thickness of 3.2 m, composed of yellow-brown clay with gravel. The gravel content is approximately 25%, with particle sizes ranging from 2–15 mm and some small rock fragments. The landslide accumulation layer with a thickness of 46.5 m, composed of yellow-brown gravelly soil. The gravel content accounts for approximately 50%, with particle sizes ranging from 3–10 cm and a rock fragment content of approximately 12%. The maximum particle size can reach 50 cm. The rock type is mainly highly weathered limestone. The sliding zone soil is yellow-brown soil with angular gravel, buried at a depth of 49.7–49.9 m, with a thickness of 0.2 m. The situation revealed by ZK2 is relatively straightforward. The sliding mass is mainly composed of fragmented rock and soil, with a significant content of fragmented rock, accounting for about 60%. The sliding zone consists of yellow-brown angular gravelly soil, with a subsurface depth ranging from 49.1 m to 49.8 m and a thickness of 0.7 m. According to the geophysical results, the electrical resistivity of the sliding zone soil revealed by the ZK1 is 316.2 Ω·m, and the shear wave velocity is 644.2 m/s (Fig. 7; Table 1).

Considering the results from the AMT, MSM, and borehole exploration, the sliding body is distributed in the frontal part of the landslide. The Deda landslide accumulation zone I is mainly composed of gravel soil, characterized by a high gravel content and loose soil structure, exhibiting features of medium to high electrical resistivity and low shear wave velocity. The bedrock of the landslide is mainly composed of limestone and sandy slate. Additionally, a fault is developed at the rear edge of the landslide, identified as a branch fault of the Chalong-ranbu fault (Fig. 8).

For the analysis of the sliding zone (Table 1), the shallow sliding zone depth detected by AMT at ZK1 is 27.5 m, and the deep sliding zone depth is 65.0 m. At ZK2 position detected by AMT, the shallow sliding zone depth is 20.2 m and the deep sliding zone depth is 68.4 m. The MSM-1 at ZK1 reveals a shallow sliding zone depth of 20.1 m and a deep sliding zone depth of 47.3 m. The MSM-2 is located at the back edge of the accumulation body, and detects a sliding depth of 36.2 m. The actual sliding zone depth revealed by drilling is 49.7 m, and at a depth of 70.9 m, a 1.6 m thick weak interlayer is exposed (Fig. 7). The actual revealed sliding zone depth at ZK2 is 49.1 m. Comparing the sliding depths revealed by AMT and MSM-1 at ZK1 with the actual revealed sliding depth at ZK1, AMT has a larger detection error, while the accuracy of MSM is higher, with a relative error of 5%. Combining drilling and MSM results, the deep sliding zone depth of the Deda I landslide (DD-I-S2) is 36.2–49.9 m. The reason for the failure to reveal the shallow sliding zone at ZK1 and ZK2 may be that the shallow sliding surface is not fully penetrated, but there are noticeable differences in physical properties. Therefore, it is speculated

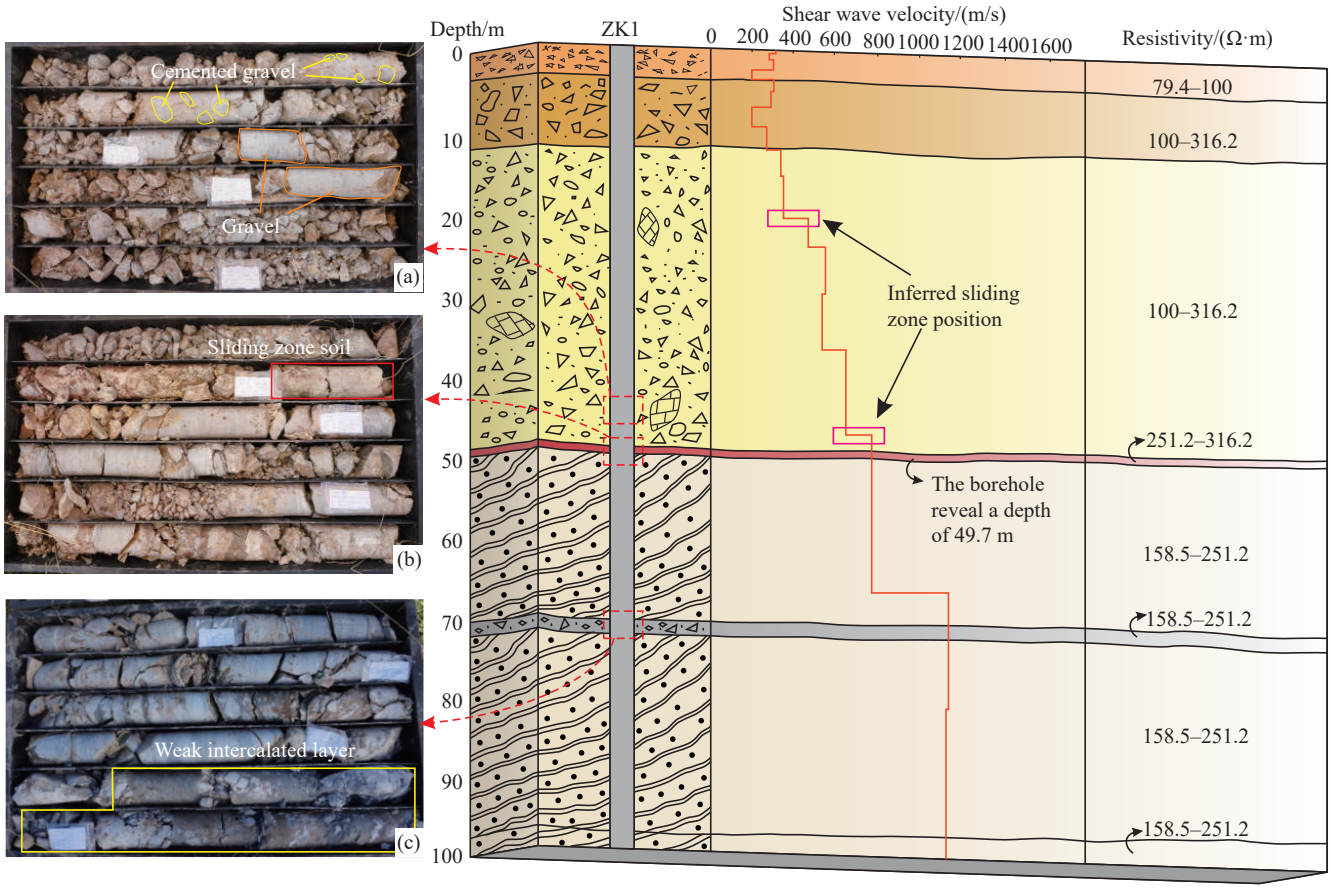

Fig. 7. Column diagram of the ZK1 borehole in the Deda ancient landslide. a–core photograph of 43.6–48.4 m; b–core photograph of 48.4–53.2 m; c–core photograph of 67.6–72.4 m.

Table 1. List of revealed sliding zone depths in Deda I landslide.

Location	ZK1	ZK2	MSM-1 at ZK1	MSM-2	AMT at ZK1	AMT at ZK2
the shallow sliding zone (DD-I-S1)/m	/	/	20.1	/	27.5	20.2
the deep sliding zone (DD-I-S2)/m	49.7	49.1	47.3	36.2	65.0	68.4

that the general burial depth of the shallow sliding zone (DD-I-S1) is 20 m.

4.3. Spatial characteristics of Deda landslide accumulation zone II

4.3.1. Results of AMT of Deda landslide accumulation zone II

From the results of AMT (Fig. 9a), it can be observed that the resistivity of the landslide accumulation ranges from 158 Ω·m to 500 Ω·m. In the case of Deda landslide accumulation zone II, only one sliding zone is detected, with a maximum burial depth of 48.2 m and an average thickness of the sliding material of 40 m, mainly consisting of gravel soil. The rear part of the landslide shows a high resistivity characteristic, with a resistivity range of 794.3–5011.8 Ω·m, indicating the electrical response of limestone. In the deep layer of the central part of the landslide, it exhibits a low resistivity characteristic, likely due to faulting and karst development. The deep layer of the front part of the landslide displays a medium to high resistivity characteristic, with resistivity values ranging from 630.9 Ω·m to 1584.8 Ω·m, suggesting the electrical response of slate and sandy slate. The revealed fault distribution pattern along this survey line is consistent with profile I-I'. Along the fault distribution, there is a low-resistance state, suggesting the possible existence of joint fracture zones in the deep rock layers, potentially leading to the formation of aquifer zones.

4.3.2. Results of MSM of Deda landslide accumulation zone II

Based on the MSM results (Fig. 9b) and a comprehensive analysis of microtremor exploration points MSM-3 and MSM-4 (Fig. 10). It is observed that the Deda landslide accumulation zone II exhibits a similar geological structure to the Deda landslide accumulation zone I, consisting of three layers: (1) shallow cover layer; (2) moderately to strongly weathered bedrock layer; (3) fresh to weakly weathered bedrock layer.

(i) Data analysis of the microtremor point MSM-3 located in the middle of the Deda II accumulation reveals the following (Fig. 10c):

Shallow cover layer: The shallow layer of the landslide mainly consists of loose gravel soil. The shear wave velocity ranges from 200.0 m/s to 543.1 m/s, with a thickness of 37.6 m.

Moderately to strongly weathered bedrock layer: The velocity ranges from 543.1 m/s to 776.7 m/s and is characterized by fragmented rock structure and loose density,

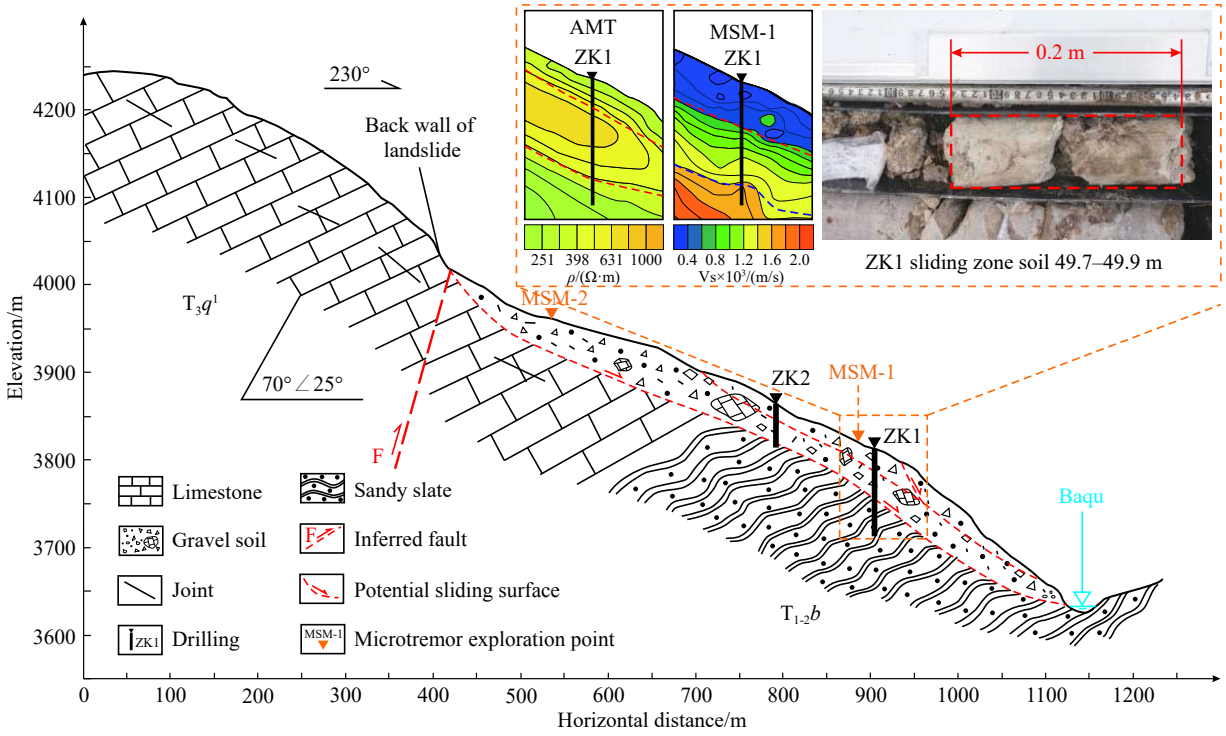

Fig. 8. Engineering geological profile I-I' for the Deda ancient landslide.

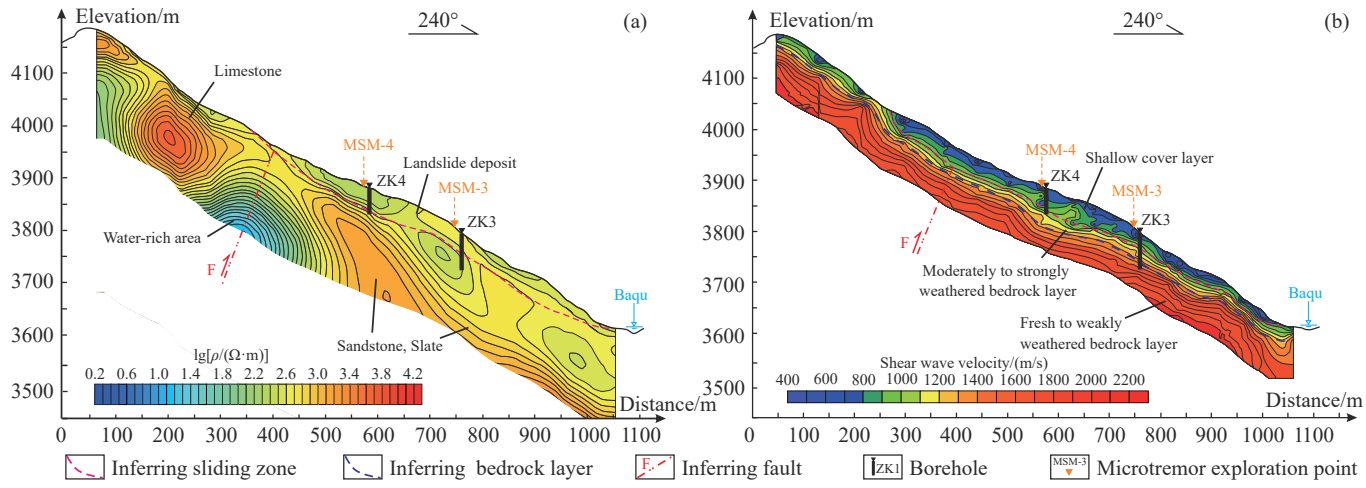

Fig. 9. Two-dimensional physical response characteristics of the II-II' sections of the Deda ancient landslide. a–Inversion results of AMT in the II-II' section of the Deda ancient landslide; b–Inversion results of MSM in the II-II' section of the Deda ancient landslide.

with a depth ranging from 37.6 m to 55.9 m and a thickness of 18.3 m.

Fresh to weakly weathered bedrock layer: The region where the shear wave velocity ranges from 776.7 m/s to 1240.8 m/s, exhibiting good rock integrity and compact structure, with a depth ranging from 55.9 m to 120.0 m with a thickness of 64.1 m.

A significant difference in shear wave velocity structure is observed at a depth of 37.6 m, with a velocity change of 218.6 m/s, indicating a potential sliding zone. The shear wave velocity of this sliding zone is 543.1 m/s.

(ii) Data analysis of the microtremor exploration point MSM-4 located in the central rear part of the Deda II accumulation reveals the following (Fig. 10f):

Shallow cover layer: The shear wave velocity in this layer ranges from 200.0 m/s to 549.1 m/s, consisting mainly of loose fragmented rocks with a thickness of 43.1 m.

Moderately to strongly weathered bedrock layer: The shear wave velocity in this layer falls between 549.1–937.1 m/s, indicating moderately to strongly weathered bedrock. It is situated at a depth of 43.1–76.8 m with a thickness of approximately 23.7 m.

Fresh to weakly weathered bedrock layer: The shear wave velocity in this zone ranges from 937.1 m/s to 1178.8 m/s, representing fresh to weakly weathered bedrock. The rock mass shows good integrity and a compact structure at a depth of 76.8–100.0 m with a thickness of approximately 23.2 m.

A significant difference in shear wave velocity structure is

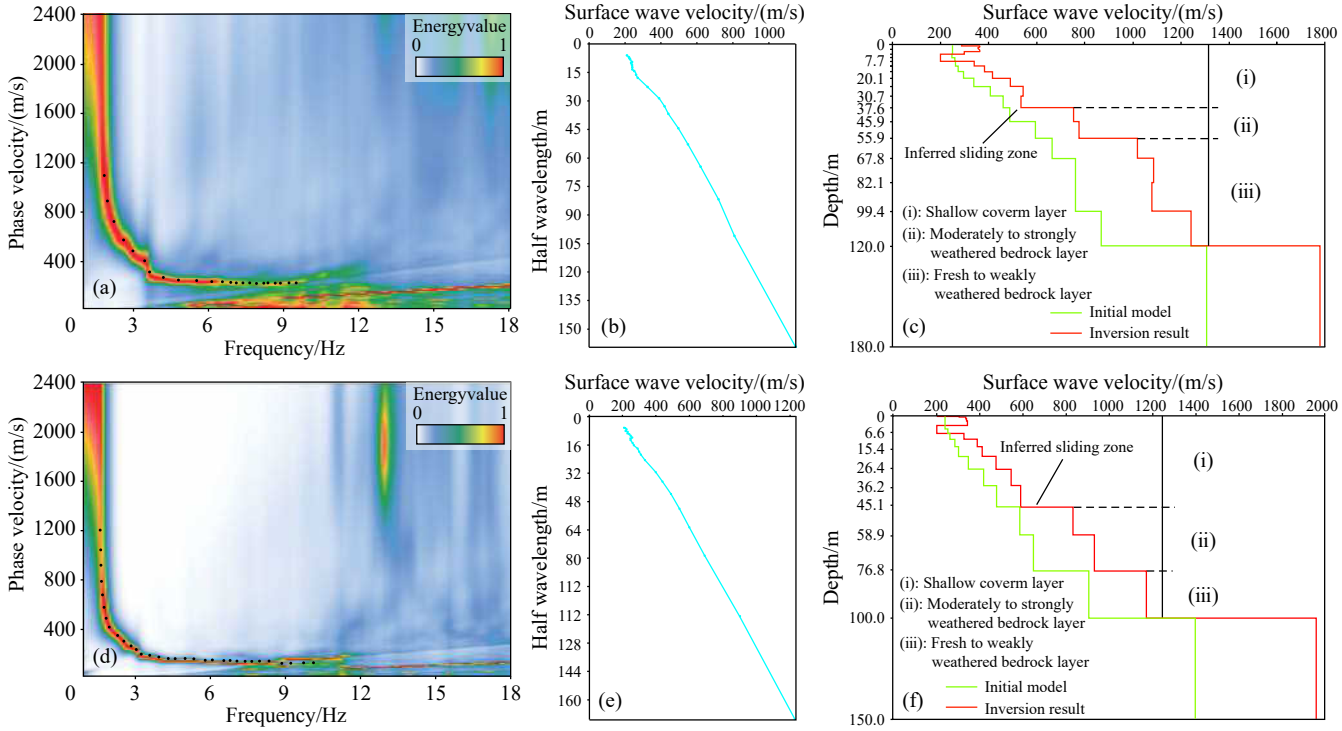

Fig. 10. Geophysical response characteristics of microtremor exploration points on Deda Ⅱ landslide. a–MSM-3 dispersion energy spectrum; b–MSM-3 dispersion curve; c–inversion of MSM-3 shear wave velocity structure; e–MSM-4 dispersion energy spectrum; f–MSM-4 dispersion curve; g–inversion of MSM-4 shear wave velocity structure.

observed at a depth of 43.1 m, with a velocity change of 288.6 m/s, indicating a potential sliding zone. The shear wave velocity of this sliding zone is 549.1 m/s.

In summary, MSM-3 reveals one sliding zone with a burial depth of 37.6 m, and MSM-4 reveals one sliding zone with a burial depth of 45.1 m. It is speculated that the sliding zone of Deda II landslide accumulation body has a burial depth of 37.6–45.1 m by MSM, with a shear wave velocity of 543.1–549.1 m/s.

4.3.3. Results of engineering geological drilling of Deda landslide accumulation zone II

For the Deda landslide accumulation zone II, borehole ZK3 and ZK4 was positioned in the central middle of the landslide accumulation to validate the geophysical survey results. And a detailed discussion of ZK3 is conducted in conjunction with the geophysical exploration results (Fig. 3a, Fig. 11). The Quaternary slope accumulation, with a thickness of 1.1 m, characterized by yellow-brown clay intermixed with angular gravel. The gravel content is approximately 30%, and the grain size ranges from 3–12 mm. The landslide accumulation, with a thickness of 37.5 m, composed of gravel soil. The gravel content is approximately 55%, with grain sizes ranging from 2–15 cm and occasional rocks up to 30 cm in size. The depth of the sliding zone ranges from 38.6–39.3 m, with a thickness of 0.7 m. The sliding zone soil is yellow-brown soil with angular gravel, with a gravel content of approximately 50% and grain sizes ranging from 2–10 mm. The sliding mass revealed by ZK4 consists of fragmented rock and soil with a thickness of 39.3 m. The exposed sliding zone is composed of completely weathered carbonaceous shale, buried at depths ranging from 39.3 m to 42.4 m. Based on the geophysical survey, the resistivity of the sliding zone soil is 410.2 Ω·m, and the shear wave velocity is 543.1 m/s (Table 2).

Combining the results from AMT, MSM, and borehole drilling, the sliding body is distributed in the frontal part of the landslide. The landslide mainly consists of gravel soil with a high gravel content and loose soil structure and exhibits characteristics of medium to high resistivity and low shear wave velocity. The bedrock of the landslide is characterized by limestone and sandy slate. Additionally, a branch fault of the Chalong-ranbu fault is observed at the rear edge of the landslide.

Considering that ZK4 is close to MSM-4, ZK4 is therefore depicted in the profile diagram for the analysis of the sliding zone (Fig. 12; Table 3). Combined drilling and geophysical results, AMT survey conducted at ZK3 revealed a sliding zone depth of 37.3 m, and at ZK4 position, the sliding depth is 44.4 m. The MSM-3 at ZK3 detects a sliding zone depth of 37.6 m, while MSM-4 at ZK4, located in the upper part of the accumulation body, detects a sliding depth of 43.1 m. The actual sliding zone depth revealed by ZK3 is 38.6 m, and at ZK4, it is 39.3 m. At ZK3 and ZK4, the sliding zone depth revealed by AMT and MSM was compared. The MSM shows higher accuracy, with relative errors of 2.6% and 1.6%. Therefore, for the sliding surface of the Deda II landslide body (DD-II-S1), the sliding zone depth is 37.6–43.1 m.

5. Discussion

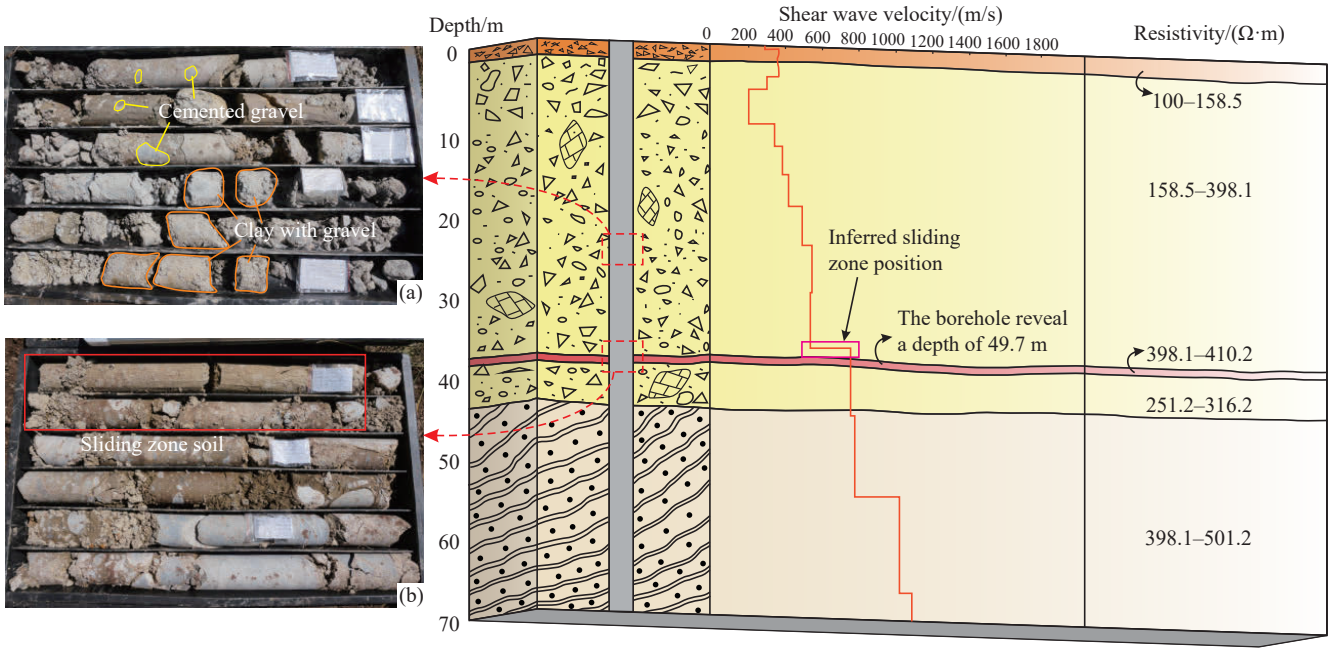

Fig. 11. Column diagram of the ZK3 borehole in the Deda ancient landslide. a–core photograph of 24.0–28.8 m; b–core photograph of 38.4–43.4 m.

Table 2. List of basic physical properties of the Deda ancient landslide.

Method	Unit	Gravel	Sliding zone	Limestone	Sandy slate
AMT	Ω·m	100–1258.9	251.2–410.2	794.3–5011.8	630.9–1584.8
MSM	m/s	200–644.2	543.1–644.2	1400–2200	1400–2200

In landslide geophysical surveys, differences in the physical properties of the landslide's spatial structure are utilized to identify its structural characteristics (Jongmans D and Garambois S, 2007; Ling CP et al., 2016; Qiu ZD et al., 2023). For example, Yang DD et al. (2021) used high-density electrical resistivity to delineate landslide shear zones (<10 Ω·m), water-rich zones (<10 Ω·m), and bedrock zones (>60 Ω·m) at the Xiashitang landslide and Xiongwa landslide in Hualong County, Qinghai Province. Faheem U et al. (2022) used electrical resistivity tomography to classify materials within the Huangnibazi landslide in Li County, Sichuan Province, into saturated soils (15–50 Ω·m), fractured zones (61–200 Ω·m) and fragmented rocks (201–1369 Ω·m) based on their electrical properties. Currently, there is limited research on the physical response characteristics of key elements in large ancient landslides, and the criteria for identifying sliding zones are not yet well established. The study is based on the application of two geophysical methods, AMT and MSM, on the Deda ancient landslide. The results indicate that AMT provides a wide range of electrical response characteristics, making it suitable for detecting underground spatial structures at great depths and large areas. It demonstrates significant advantages in identifying landslide thickness, sliding zone depth, fault distribution, and karst development. However, the accuracy of shallow layer detection is relatively low. On the other hand, MSM distinguishes subsurface structures and shows high precision in identifying shallow cover layers, but the accuracy of deep and large-scale geological structure detection is insufficient. For large-scale deep-seated landslides in the alpine canyons of the eastern Tibetan Plateau, a combination of two methods can be employed, complementing, and validating each other, to effectively study the spatial structural characteristics of landslides.

The research on the detection accuracy of MSM in spatial structures has gained widespread application and recognition among scholars. Xu PF et al. (2021) employed MSM for exploration of the Guangzhou subway routes, interpreting bedrock interfaces and highly weathered layer interfaces. When compared with the actual depths revealed by drilling, the maximum relative error was 5.46%. Zhang RH et al. (2020) applied the micro-movement H/V spectral ratio method to interpret the depth of soil-rock interfaces, and the average error compared to drilling disclosure depths was 4.33%.

Therefore, the study proposes a method for identifying sliding zones based on MSM. This method involves identifying regions of different shear wave velocities in the subsurface layers. In this study, the sliding zone soil had shear wave velocities ranging from 543.1–644.2 m/s, indicating a low shear wave velocity state. In contrast, the velocities in the bedrock reached a high shear wave velocity state of 1400–2200 m/s. Furthermore, the velocities remained relatively stable at certain depths after the velocity transition. Using this information, the interface between these velocity states can be inferred as the sliding zone location. Through data analysis of microtremor exploration points MSM-1, MSM-3 and MSM-4 on the Deda landslide, the shear zone depths revealed by MSM were 47.3 m, 37.5 m and 43.1 m respectively, while the depths revealed by drilling were 49.7 m, 38.6 m and 42.4 m respectively. The relative errors were

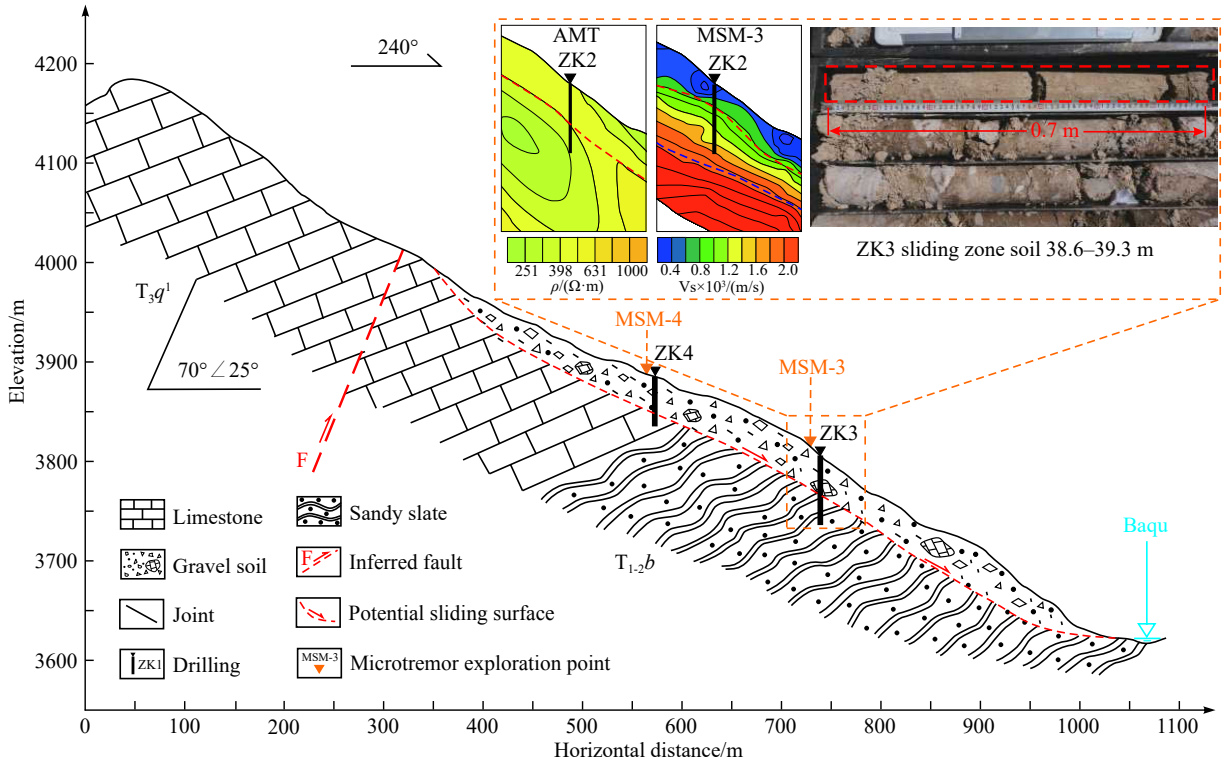

Fig. 12. Engineering geological profile II-II' for the Deda ancient landslide.

Table 3. List of revealed sliding zone depths in Deda II Landslide.

Location	ZK3	ZK4	MSM-3 at ZK3	MSM-4 at ZK4	AMT at ZK3	AMT at ZK4
the sliding zone (DD-I-S1)/m	38.6	42.4	37.6	43.1	37.2	44.4

5.0%, 2.6% and 1.6% demonstrating that the identification error of the sliding zone is within 5% using MSM. This indicates that MSM has high precision and a low error rate, making it suitable for identifying the spatial structure of sliding zones.

6. Conclusions

The study focused on the Deda ancient landslide and employed methods such as field investigations, geophysical prospecting, and engineering geological drilling to investigate its spatial structural features. The results and findings were concluded as the following.

(i) The Deda landslide is a large ancient landslide, which can be divided into three parts in plan: The Deda landslide accumulation zone I, the Deda landslide accumulation zone II and the source zone of the Deda ancient landslide (III). Based on the interpretation of AMT and MSM, it is observed that the Deda I landslide exhibits two sliding zones. The Deda II landslide features a single sliding zone. The resistivity values of the sliding zones range from 251.2 Ω·m to 410.2 Ω·m, and the shear wave velocities range from 543.1 m/s to 644.2 m/s.

(ii) Integrating geophysical and drilling results, the shallow sliding zone (DD-I-S1) depth of the Deda I landslide is approximately 20 m, and the deep sliding zone (DD-I-S2) depth is 36.2–49.9 m. The volume of the Deda I landslide is 8.7×10^6 m^3–12.0×10^6 m^3. The sliding zone (DD-II-S1) depth of the Deda II landslide is 37.6–43.1 m. The volume of the Deda II landslide is 9.4×10^6–10.8×10^6 m^3.

(iii) The MSM has high resolution within the shallow range and is sensitive to the spatial structure of sliding zones, the landslide mass, and bedrock. The AMT is effective in detecting the characteristics of deep-seated rock and soil. It is suitable for detecting underground spatial structures on a large scale and is advantageous in revealing the distribution of faults and karst regions. In the alpine canyon areas of the eastern Tibetan Plateau, the combined application of AMT and MSM is advantageous for achieving a detailed investigation of the depth and accuracy of landslide spatial structure. This provides reliable technical support for significant engineering construction in the region.

(iv) A sliding zone identification model based on MSM is proposed in this study. By analyzing the abrupt changes in shear wave velocity and the subsequent stability of wave velocity within a certain depth, the preliminary position of the sliding zone can be inferred. By applying this model to analyze the results of microtremor points MSM-1, MSM-3 and MSM-4, the relative errors of the sliding zone depths identified by MSM and those revealed by drilling are within 5%.

CRediT authorship contribution statement

Zhen-dong Qiu and Chang-bao Guo devised the study plan and wrote the paper. Zhen-dong Qiu conducted data processing and analysis; Zhi-hua Yang, Rui-an Wu and Yi-ying Zhang participated in the field investigation; Yi-qiu Yan, Feng Jin and Wen-kai Chen conducted comprehensive

analysis and image processing.

Declaration of competing interest

The authors declare no conflicts of interest.

Acknowledgements

This study was supported by the National Natural Science Foundation of China (42372339) and the China Geological Survey Project (DD20221816, DD20190319). The field geophysical prospecting and data processing of this work were guided and assisted by senior engineer Guo-hua Zhang of Chengdu Blue Sky Information Engineering Co., Ltd.; the field engineering drilling construction was guided and assisted by senior engineers Chang-li Wei and Wei Liao of Sichuan Geological Survey Institute; postgraduate student Ji-jun Jin from the Institute of Geomechanics, Chinese Academy of Geological Sciences and postgraduate student De-guang Song from Tibet University provided relevant help and support in this field survey; postgraduate students Yu-wei Ling and Xin-xia Yuan from China University of Geosciences (Wuhan) participated in some map drawing work.

References

Aki K. 1957. Space and time spectra of stationary stochastic waves, with special reference to microtremors. Bulletin of the Earthquake Research Institute, 35, 415–456.

Cagniard L. 1953. Basic theory of the magneto-telluric method of geophysical prospecting. Geophysics, 18(3), 605–635. doi: 10.1190/1.1437915.

Capon J. 1969. High-resolution frequency-wavenumber spectrum analysis. Proceedings of the IEEE, 57(8), 1408–1418. doi: 10.1109/PROC.1969.7278.

Cruden DM, Varnes DJ. 1996. Landslide types and processes, special report, transportation research board. Proceedings of the National Academy of Sciences of the United States of America, 247, 36–75.

China Earthquake Administration (CEA). 2015. Seismic Ground Motion Parameters Zonation Map of China (GB 18306-2015). Seismological Press, Beijing. (in Chinese with English Abstract)

Dewey JF, Shackleton RM, Chang CF, Sun YY. 1988. The tectonic evolution of the Tibetan Plateau. philosophical transactions of the Royal Society of London. Series A, Mathematical and Physical Sciences, 327, 379–413. doi: 10.1098/rsta.1988.0135.

Di QY, Xue GQ, Zeng QD, Wang ZX, An ZG, Lei D. 2020. Magnetotelluric exploration of deep-seated gold deposits in the Qingchengzi orefield, Eastern Liaoning (China), using a SEP system. Ore Geology Reviews, 122, 103501. doi: 10.1016/j.oregeorev.2020.103501.

Faheem U, Su LJ, Li C, Liu ZY, Hu BL. 2022. Geophysical prospecting related to earthflow reactivation and hazard assessment: a study based on Huangnibazi slope failure in Sichuan Province, China. Bulletin of Engineering Geology and the Environment, 81, 1–14. doi: 10.1007/s10064-021-02525-7.

Guo CB, Zhang YS, Montgomery DR, Du YB, Zhang GZ, Wang SF. 2016. How unusual is the long-runout of the earthquake-triggered giant Luanshibao landslide, Tibetan Plateau, China? Geomorphology, 259, 145–154. doi: 10.1016/j.geomorph.2016.02.013.

Guo CB, Yan YQ, Zhang YS, Zhang JX, Zheng YZ, Li X, Yang ZH, Wu RA. 2021. Study on the creep-sliding mechanism of the giant Xiongba ancient landslide based on the SBAS-InSAR method, Tibetan Plateau, China. Remote Sensing, 13(17), 3365. doi: 10.3390/rs13173365.

Guo CB, Yan YQ, Zhang YS, Wu RA, Yang ZH, Li X, Ren SS, Zhang YY, Wu ZK, Liu JX. 2022. Research progress and prospect of failure mechanism of large deep-seated creeping landslides in Tibetan Plateau, China. Earth Science, 47(10), 3677–3700. doi: 10.3799/dqkx.2022.249.

Guo CB, Zhang YS, Yuan H, Liu DT, Yan YQ, Hua S, Ren SS. 2023. Study of an ancient landslide reactivation mechanism based on centrifuge model testing: An example of the Jiangdingya ancient landslide reactivation in 2018, Gansu Province, China. Landslides, 20(1), 127–141. doi: 10.1007/s10346-022-01978-5.

Gao WW, Gao W, Hu RL, Xu PF, Xia JG. 2018. Microtremor survey and stability analysis of a soil-rock mixture landslide: A case study in Baidian town, China. Landslides, 15, 1951–1961. doi: 10.1007/s10346-018-1009-x.

Jongmans D, Garambois S. 2007. Geophysical investigation of landslides: A review. Bulletin de laSociete Geologique de France, 178(2), 101–112. doi: 10.2113/gssgfbull.178.2.101.

Le Roux O, Jongmans D, Kasperski J, Stéphane S, Potherat P, Lebrouc V, Lagabrielle R, Meric O. 2011. Deep geophysical investigation of the large Séchilienne landslide (Western Alps, France) and calibration with geological data. Engineering Geology, 120(1-4), 18–31. doi: 10.1016/j.enggeo.2011.03.004.

Louie JN, Faster B. 2001. Shear wave velocity to 100 meters depth from refraction microtremor analysis. Bulletin of the Seismological Society of America, 91(2), 347–364 doi: 10.1785/0120000098.

Li X, Liao QL, Wang SJ, Liu JS, Lee S. 2008. On evaluating the stability of the Baiyian ancient landslide in the three gorges reservoir area, Yangtze River: A geological history analysis. Environmental Geology, 55(8), 1699–1711. doi: 10.1007/s00254-007-1121-z.

Ling CP, Xu Q, Zhang Q, Ran JX, Lv HB. 2016. Application of electrical resistivity tomography for investigating the internal structure of a translational landslide and characterizing its groundwater circulation (Kualiangzi landslide, Southwest China). Journal of Applied Geophysics, 131, 154–162. doi: 10.1016/j.jappgeo.2016.06.003.

Ma N, Wang GW, Kamai T, Doi I, Chigira M. 2019. Amplification of seismic response of a large deep-seated landslide in Tokushima, Japan. Engineering Geology, 249, 218–234. doi: 10.1016/j.enggeo.2019.01.002.

Molnar S, Sirohey A, Assaf J, Bard PY, Castellaro S, Cornou C, Cox B, Guillier B, Hassani B, Kawase H, Matsushima S, Sánchez-Sesma FJ, Yong A. 2022. A review of the microtremor horizontal-to-vertical spectral ratio (MHVSR) method. Journal of Seismology, 26(4), 653–685. doi: 10.1007/s10950-021-10062-9.

Naudet V, Lazzar IM, Perrone A, Loperte A, Piscitelli S, Lapenna V. 2008. Integrated geophysical and geomorphological approach to investigate the snowmelt-triggered landslide of Bosco Piccolo village (Basilicata, southern Italy). Engineering Geology, 98(3-4), 156–167. doi: 10.1016/j.enggeo.2008.02.008.

Okada H, Suto K. 2003. The Microtremor Survey Method. Society of Exploration Geophysicists. doi: 10.1190/1.9781560801740.ch3.

Peng JB, Ma RY, Lu QZ, Li X, Shao TQ. 2004. Geological hazards effects of uplift of Qinghai Tibet Plateau. Advances in Earth Science, 2004(03), 457–466. doi: 10.11867/j.issn.1001-8166.2004.03.0457.

Qiu ZD, Guo CB, Yang ZH, Wu RA, Yan YQ, Zhang YY, Jin F, Chen WK. 2023. Research on the spatial structure characteristics and formation mechanism of the Deda ancient landslide based on Microtremor Survey Method in Sichuan province, China. Journal of Geomechanics. doi: 10.12090/j.issn.1006-6616.2023183. (in Chinese with English Abstract)

Su LJ, Xu XQ, Geng XY, Liang SQ. 2017. An integrated geophysical approach for investigating hydro-geological characteristics of a debris landslide in the Wenchuan earthquake area. Engineering Geology, 219, 52–63. doi: 10.1016/j.enggeo.2016.11.020.

Tikhonov AN. 1950. Determination of the electrical characteristics of the deep strata of the earth's crust. Doklady Akadamia Nauk. 73(2), 295–311.

Tian BQ, Du YN, You ZW, Zhang RH. 2019. Measuring the sediment thickness in urban areas using revised H/V spectral ratio method. Engineering Geology, 260, 105223. doi: 10.1016/j.enggeo.2019.105223.

Wu RA, Guo CB, Ni JW, Song DG, Zhan WW, Zhong N, Yang ZH, Li X, Yan YQ. 2023. Ancient landslide river damming event in the Batang fault zone, Tibetan Plateau. Bulletin of Engineering Geology and the Environment, 82, 25. doi: 10.1007/s10064-022-03048-5.

Xu JR, Zhao ZX. 2009. Extensional seismogenic stress and tectonic movement on the central region of the Tibetan Plateau. International Journal of Geophysics, 2009, 1–8. doi: 10.1155/2009/897424.

Xu PF, Ling SQ, Long G, Qiao GQ, Shen QH, Yao J, Zhang H. 2021. ESPAC-based 2D mini-array microtremor method and its application in urban rail transit construction planning. Tunnelling and Underground Space Technology, 115, 104070. doi: 10.1016/j.tust.2021.104070.

Xu Q, Zhao B, Dai KR, Dong XJ, Li WL, Zhu X, Yang YH, Xiao XX, Wang X, Huang J, Lu HY, Deng B, Ge DQ. 2023. Remote sensing for landslide investigations: A progress report from China. Engineering Geology, 107156. doi: 10.1016/j.enggeo.2023.107156.

Yang DD, Qiu HJ, Zhu YR, Liu ZJ, Pei YQ, Ma SY, Du C, Sun HS, Liu Y, Cao MM. 2021. Landslide characteristics and evolution: What we can learn from three adjacent landslides. Remote Sensing, 13(22), 4579. doi: 10.3390/rs13224579.

You ZW, Xu PF, Qian J, Cao LP, Du YN, Fu Q. 2022. Frequency-bessel transform based microtremor survey method and its engineering application. International Journal of Environmental Research and Public Health, 19(20), 13484. doi: 10.3390/ijerph192013484.

Yan YQ, Guo CB, Zhong N, Li X, Li CH. 2022. Deformation characteristics of Jiaju ancient landslide based on InSAR monitoring method, Sichuan, China. Earth Science, 47(12), 4681–4697. doi: 10.3799/dqkx.2022.162.

Yang XH, Jiang YW, Zhu JC, Ding BY, Zhang WX. 2023. Deformation characteristics and failure mechanism of the Moli landslide in Guoye Town, Zhouqu County. Landslides, 20(4), 789–800. doi: 10.1007/s10346-022-02019-x.

Yang ZH, Guo CB, Wu RA, Shao WW, Yu PF, Li CH. 2023. Potential seismic landslide hazard and engineering effect in the Ya'an-Linzhi section of the Sichuan-Tibet transportation corridor, China. China Geology, 6, 228–240. doi: 10.31035/cg2023032.

Yu PL, Qu T, He RL, Liu JL, Wang SF, Chen XL. 2023. Application of tensor CSAMT with high-power orthogonal signal sources in Jiama porphyry copper deposit, South Tibet. China Geology, 6, 37–49. doi: 10.31035/cg2021065.

Zhou RJ, Chen GX, Li Y. 2005. Research on active faults in Litang Batang region western Sichuan province, and the seismogenic structures of the 1989 Batang Ms 6. 7 earthquake swarm. Seismology and Geology, 27(1), 31–43(in Chinese with English Abstract).

Zhang RH, Xu PF, Ling SQ, Du YN, You ZW, Wang ZH, Sun CY. 2020. Detection of the soil-rock interface based on microtremor H/V spectral ratio method: A case study of the Jinan urban area. Chinese Journal of Geophysics, 63(01), 339–350 (in Chinese with English Abstract) doi: 10.6038/cjg2020M0678.

Zhang YS, Guo CB, Lan HX, Zhou NJ, Yao X. 2015. Reactivation mechanism of ancient giant landslides in the tectonically active zone: a case study in Southwest China. Environmental Earth Sciences, 74, 1719–1729. doi: 10.1007/s12665-015-4180-6.

Zhang LQ. 2017. Study on Deformation of Faults in Batang Region in Western Sichuan. Chengdu, Chengdu University of Technology, Ph. D thesis, 20–24 (in Chinese with English Abstract).

Zhang YY, Guo CB, Yang ZH, Wu RA, Yan YQ, Xu ZX, Wang ZW. 2021. Development characteristics and reactivation trend of Zhama ancient landslide in Batang, Sichuan. Geological Bulletin of China, 40(12), 2002–2014(in Chinese with English Abstract).

Zhang SL, Yin YP, Hu XW, Wang WP, Li ZL, Wu XM, Luo G, Zhu SN. 2021. Geo-structures and deformation-failure characteristics of rockslide areas near the Baige landslide scar in the Jinsha River tectonic suture zone. Landslides, 18, 3577–3597. doi: 10.1007/s10346-021-01741-2.